

The Impact on a GCM Climate of an Extended Mosaic Technique for the Land–Atmosphere Coupling

ANDREA MOLOD

Department of Earth and Planetary Sciences, The Johns Hopkins University, Baltimore, Maryland

HAYDEE SALMUN

Department of Geography, Hunter College, City University of New York, New York, New York

DARRYN W. WAUGH

Department of Earth and Planetary Sciences, The Johns Hopkins University, Baltimore, Maryland

(Manuscript received 1 October 2003, in final form 29 March 2004)

ABSTRACT

Heterogeneities in the land surface on scales smaller than the typical general circulation model (GCM) grid size can have a profound influence on the grid-scale mean climate. There exists observational and modeling evidence that the direct effects of surface heterogeneities may be felt by the atmosphere well into the planetary boundary layer. The impact of including an “extended mosaic” (EM) scheme, which accounts for the vertical influence of land surface heterogeneities in a GCM, is evaluated here by comparing side-by-side GCM simulations with EM and with the more standard mosaic formulation (M).

Differences between the EM and M simulations are observed in the boundary layer structure, in fields that link the boundary layer and the general circulation, and in fields that represent the general circulation itself. Large EM – M differences are found over the eastern United States, eastern Asia, and southern Africa in the summertime, and are associated with a boundary layer eddy diffusion feedback mechanism. The feedback mechanism operates as a positive or negative feedback depending on the local Bowen ratio. Significant EM – M differences are also found in the region of the Australian monsoon and in the strength of the stationary Pacific–North America pattern in the northern Pacific.

1. Introduction

The character of the land surface is highly variable, as has been shown clearly by Land Remote Sensing Satellite (Landsat) and other visible imagery. The heterogeneity of the land surface exists over a wide range of spatial scales that are determined by the variability of vegetation cover, the types of terrain, soil texture and wetness, the amount of cloud cover, and the extent of urban areas. The scale of these heterogeneities is typically smaller, and in some cases much more so, than the characteristic grid scale in most current general circulation models (GCMs) used in climate studies. The heterogeneities on scales smaller than the typical grid scale in current global climate models together with the difficulty of capturing the impact of the subgrid-scale variability on the grid scale presents a challenge to properly modeling the role of the land surface in GCMs.

The majority of the GCMs that are participating in the Atmospheric Model Intercomparison Project (AMIP) II (Gates 1995) account for the subgrid-scale variability and its impact on the atmospheric boundary layer by specifying soil and vegetation parameters that represent a “composite” vegetated surface and its underlying soil for each GCM grid square. A few GCMs (e.g., Rosenzweig and Abramopoulos 1997; Ducoudre et al. 1993; Koster and Suarez 1992a) account for the subgrid-scale heterogeneity using a “mosaic” approach, in which separate heat and moisture balance equations are solved for each vegetation type contained within a GCM grid square, and the resulting heat and moisture fluxes are aggregated to describe the coupling to the atmospheric boundary layer.

Scaling arguments and observations (see e.g., Mahrt 2000; Angevine et al. 2003; Hubbe et al. 1997) suggest that the direct effects of the heterogeneities are present at heights that extend well into the planetary boundary layer (PBL). The composite approach does not allow for the direct propagation of the independent characteristics of each vegetation type into the atmosphere at

Corresponding author address: Dr. Andrea Molod, Department of Earth, Atmospheric and Planetary Sciences, MIT, Cambridge, MA 02139.
E-mail: molod@ocean.mit.edu

all, and the mosaic technique does not account for the direct vertical influence of the land surface heterogeneities beyond the height of the surface layer. The limits on the vertical influence of surface heterogeneities imposed by these techniques may well constitute an important limitation to capturing the effectiveness of the communication between the land surface heterogeneity and the atmosphere (Mahrt 2000).

Koster and Suarez (1992b) discuss and evaluate some of the assumptions and limitations of the mosaic approach. One of the assumptions made in the Koster–Suarez implementation of mosaic when computing the surface–atmosphere gradients is that the atmospheric reference level may be taken as the surface layer height, and that the overlying atmosphere at this level is uniform over the grid square. They recognize, however, that as the length scale of horizontal heterogeneity increases, the atmosphere overlying each scene type is expected to retain its distinct character to higher levels. The mosaic approach, therefore, underestimates the variability of the gradients (and therefore the turbulent fluxes) at and above the surface layer.

Other studies have also addressed the limitations of mosaic as regards the vertical extent of the influence of surface heterogeneities. The concept of a blending height, discussed in the literature (summarized in Mahrt 2000) as the level at which the atmosphere above a heterogeneous terrain becomes horizontally homogeneous, was applied to GCM scales and parameterizations in Bringfelt et al. (1999), where they explicitly state that mosaic assumes that the blending height is at the surface layer, and that this might not be an adequate representation of the impact of surface heterogeneity. This limitation of mosaic was also suggested by the results of the study by Mölders et al. (1996), where the differences between mosaic and an explicit subgrid-scale model were small in the middle to upper troposphere and increased with proximity to the surface starting just inside the atmospheric boundary layer.

An attempt to address the issue of assuming a uniform atmosphere at the reference level and the possibility that the blending height may be above this level was presented by Arola (1999), making use of a technique originally proposed by Vihma (1995). The reference-level temperature, moisture, and winds were approximated as functions of the different vegetation types, and as a result the blending height is raised to the level of the surface layer (not below). This extension of the standard mosaic approach (not to be confused with the “extended mosaic” approach being examined in the present study) was presented as an improvement over the standard mosaic approach.

A technique called *extended mosaic* (EM) was presented in Molod et al. (2003), which overcomes the limitations of mosaic discussed earlier and allows the impact of aggregation effects of subgrid-scale variability to extend throughout the vertical extent of the planetary boundary layer where conditions warrant. Ex-

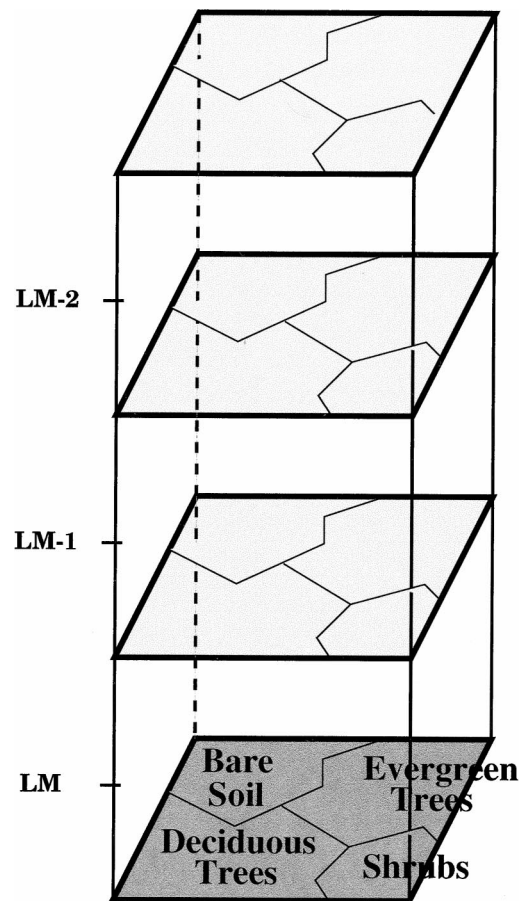


FIG. 1. Schematic of the extended mosaic technique 1. Here, LM refers to the lowest model level.

tended mosaic is a modification of the standard mosaic technique to model the coupling between the heterogeneous land surface and the turbulent planetary boundary layer. Extended mosaic follows the mosaic approach in that the surface energy equations are solved separately for each tile or vegetation type in a grid box, but extends the direct influence of surface heterogeneities upward throughout the entire depth of the turbulent atmospheric boundary layer by performing the entire turbulent boundary layer calculation in tile space (Fig. 1). As in the existing mosaic approach, the tiles of the mosaic interact only through the influence on the grid-scale atmospheric fields. The essence of this technique, therefore, is the interplay between processes that occur in GCM grid space and processes that occur in “tile space,” and the extension of that interplay throughout the depth of the turbulent layer.

The present study evaluates a set of GCM experiments that compare EM to the standard mosaic (M) technique. The fundamental issues that the EM and M experiments are designed to address relate to the impact on boundary layer processes and the links to the mean climate. The model is presented briefly in section 2a,

followed by a description of the experiments in section 2b. The presentation of the results begins in section 3 with global maps of the ensemble mean differences between the seasonal mean EM and M simulations, which provide an overview of the general behavior and impact of the modeling technique on the simulated climate. The behavior of the simulations in regions of interest are then examined in more detail in section 4, with additional focus on the simulated physical processes underlying the differences. A discussion of the direct connection between the change in modeling technique and the differences seen in the GCM simulations follows in section 5. The study is summarized in section 6, which also includes a discussion of future work that is beyond the scope of the present study, with a focus on the validation of EM using observations.

2. Model description and GCM experiments

a. Relevant GCM parameterizations

Extended mosaic is the technique used in the Goddard Earth Observing System (GEOS) GCM to provide the coupling between the GCM parameterizations for turbulence and for land surface processes. The vertical regime in the GEOS GCM is divided into the free atmosphere, the planetary boundary layer (implicitly), the surface layer, and the viscous sublayer, all above the land or ocean surface. The vertical resolution is variable, and there are 8–10 layers inside the PBL, with the thinnest layers near the ground approximately 20–30 m thick. The turbulence parameterization consists of an element that handles the vertical diffusion above the surface layer using a second-order (or 1.5 order) closure scheme (Helfand and Labraga 1988; Helfand et al. 1999), and an element that handles the turbulent fluxes of heat, moisture, and momentum in the surface layer and viscous sublayer (Helfand and Schubert 1995). The Helfand and Labraga scheme was modified by Helfand et al. (1999) to include a “moist turbulence” scheme to simulate the effects of the vapor-to-liquid phase change on the buoyancy, and therefore on the source of turbulent kinetic energy as well.

The GEOS GCM land surface processes are parameterized using the mosaic Soil–Vegetation–Atmosphere–Transfer model (SVAT) developed by Koster and Suarez (1992a,c, hereafter KS-LSM). The deep soil temperature, canopy temperature, three soil moisture layers, a canopy interception reservoir, a canopy air specific humidity, and a snowpack are predicted and retained separately for each vegetation “tile” in a grid square. The subgrid-scale variability of the surface is modeled using a mosaic approach, in which the surface energy and moisture transfers in the surface layer and soil are computed separately for each tile that makes up the mosaic.

b. GCM experiments

The experiments described here are designed to examine the impact on a GCM’s climate of modeling the influence of subgrid-scale heterogeneity in vegetation using the extended mosaic technique. Two 10-yr simulations were performed with the GEOS GCM, one coupling the turbulence and land surface schemes with EM and one using the standard mosaic (M) coupling. The M simulation was performed with a modified version of the EM code that explicitly aggregates the turbulent fluxes at the surface layer. Constructing the experiments in this manner ensures that the *only* differences between the GCM simulations are due to the choice of the level in the vertical at which the turbulent fluxes are aggregated.

Each simulation (EM and M) began with the same initial conditions, and the deep-soil state was spun up from 8 yr of assimilation with the GEOS data assimilation system (DAS) using EM. The boundary conditions at the sea surface [sea surface temperature (SST) and sea ice extent] were specified from the climatological data of Reynolds (1988). Due to the inherent or internal variability of the GCM simulations (which may mimic the variability of the earth’s climate), it is important to assess the statistical significance of the differences that will be examined here. Because the boundary conditions are specified from the (same) climatological conditions, the year-to-year differences within each simulation are due mainly to the atmospheric and soil state at the beginning of the year, and the 10 years of the simulation may be regarded statistically as a 10-member ensemble of simulations. The presence of variability on scales greater than 1 yr would generate some correlation between the initial states of the ensemble members, but this is assumed not to interfere with the ability to sufficiently sample the phase space of initial states that is needed to constitute a proper ensemble. If the results of the 10-member ensemble of the EM experiment are a sample from the population of the simulated climate of the GCM using EM, and the M experimental results are also a sample from a population, then a Student’s *t* test can be performed to test the differences in the mean of the two samples to determine the probability that they were taken from two different populations. The EM – M results to be presented here were tested in this manner and the null hypothesis that the means of the EM and M samples are from the same population was rejected with a 70%–80% level of significance.

3. Results: Global perspective

a. Boundary layer structure

The fields chosen here as indicators of the vertical structure of the boundary layer turbulence are the planetary boundary layer depth, the vertical fluxes of heat and moisture at the surface layer, and the canopy tem-

perature. The PBL depth, which is defined as the GCM level at which the turbulent kinetic energy decays below 10% of its maximum value in the air column, depends primarily on the boundary conditions at the surface, which include the temperature, moisture, and turbulent fluxes of each, and on the vertical extent of the turbulent diffusion of buoyancy, momentum, and turbulent kinetic energy. The impact on the simulated boundary layer structure of choosing extended mosaic or mosaic will be manifest in the differences in PBL depth between the two simulations. The latent and sensible heat fluxes at the surface, in addition to providing the boundary condition for the vertical flux of heat and moisture in the atmosphere, are both central terms in the energy budget at the surface, which is primarily a result of the balance between the net radiation and the turbulent fluxes. The net radiation at the surface is primarily affected by the surface albedo, the atmospheric water vapor levels, the surface temperature, and the cloud cover, all of which are not *directly* altered by performing the simulations with the extended mosaic versus the mosaic technique. The net radiation balance will therefore not be presented here. The surface turbulent fluxes of heat and moisture are directly affected by the choice of modeling technique and are a focus of the analysis. The net result of the surface energy balance can be seen by examining the ensemble mean canopy temperature. EM – M differences in ensemble seasonal means of the indicators of the boundary layer structure are shown in Fig. 2.

The ensemble mean June–July–August (JJA) and December–January–February (DJF) planetary boundary layer depth EM – M differences are shown in Figs. 2a and 2b. Although the seasonal mean EM – M difference does not reflect the amplitude of the diurnal cycle of the PBL depth, this measure reflects the difference in daily maximum PBL depth between the EM and M simulations. Over land areas, the differences in PBL depths are larger in the summertime, when the PBL depth itself is higher. The PBL is higher in EM than in M by up to 200 m over much of the North and South American continents in JJA, and by up to 100 m over those regions in DJF. These differences are on the order of 10% of the PBL height values. The PBL depths are also higher in EM over Africa in the summertime, over central Africa during JJA and southern Africa during DJF, and over southeastern Asia and the Indian subcontinent in JJA. The land areas where the PBL is lower in the EM simulation are northern China and Mongolia in JJA, central Canada in JJA, and the Mideastern deserts and parts of northern Europe. The largest EM – M differences in PBL depth over the oceans are in the regions of the wintertime storm tracks, near 45°N latitude in DJF and 45°S latitude in JJA, and the general trend over the oceans is for higher PBL depths in the EM simulation. The behavior of the ensemble mean sensible heat flux, Figs. 2e and 2f, can be described by its similarity

to the behavior of the PBL height over the continents, but shows small differences over the oceans.

The ensemble mean EM – M differences in latent heat flux are shown in Figs. 2c and 2d. The largest EM – M differences in latent heat flux over the land surface are in the summer hemisphere, and generally in the regions where there were also large differences in PBL height. The latent heat fluxes are smaller by up to 15 W m^{-2} in the EM simulation over the eastern United States, the Indian subcontinent, and southern Africa in the summer, where the mean values of latent heat flux in EM are up to 90 W m^{-2} (not shown). These are the regions where the PBL depth in EM is higher. The latent heat fluxes are larger in EM over eastern Asia, central Canada, and central South America. The EM – M latent heat flux difference over the ocean, for GCM simulations in which the sea surface temperature is specified, depends predominantly on the surface wind speed and on the humidity of the overlying air mass. These differences over the oceans, such as the large difference south and east of Australia in JJA, are therefore not a direct result of changing the modeling technique for the land–atmosphere coupling, but reflect nonlocal effects and are due to the feedbacks with the atmosphere.

The ensemble mean JJA and DJF EM – M differences in T_c are shown in Figs. 2g and 2h. The orange and yellow areas over the United States during JJA and over southeastern Africa in DJF indicate summertime regions where the EM simulation has a canopy temperature that is warmer than the M simulation by up to 2 K. These are regions mentioned earlier where the summertime PBL height and sensible heat flux are higher in the EM simulation than in the M simulation, and the latent heat flux is reduced. There is no such correspondence between T_c , PBL height, and surface fluxes in the winter season. The EM canopy temperatures are also warmer than M by up to 2 K over western and northeastern Canada and over the northwestern United States in DJF. The behavior of the canopy temperature in these regions does not correspond to the behavior of the PBL height or surface fluxes, suggesting a remote influence that will be elaborated in section 3c. The regions where the EM simulation is colder than M by 1 K or more, shaded in dark blue, include most of the area covered by glacial or sea ice, and an area in eastern Asia across northern China and Mongolia, corresponding to the Asian region where the PBL height and sensible heat flux are reduced in EM.

b. Links to the global climate

The most important processes of communication between the boundary layer and the overlying troposphere are cumulus convection and frontal convection, whereby boundary layer air, with its moisture, momentum, and turbulent kinetic energy, is vented aloft. A suitable proxy for the magnitude of the occurrence of either one of these processes is the precipitation field or total cloud

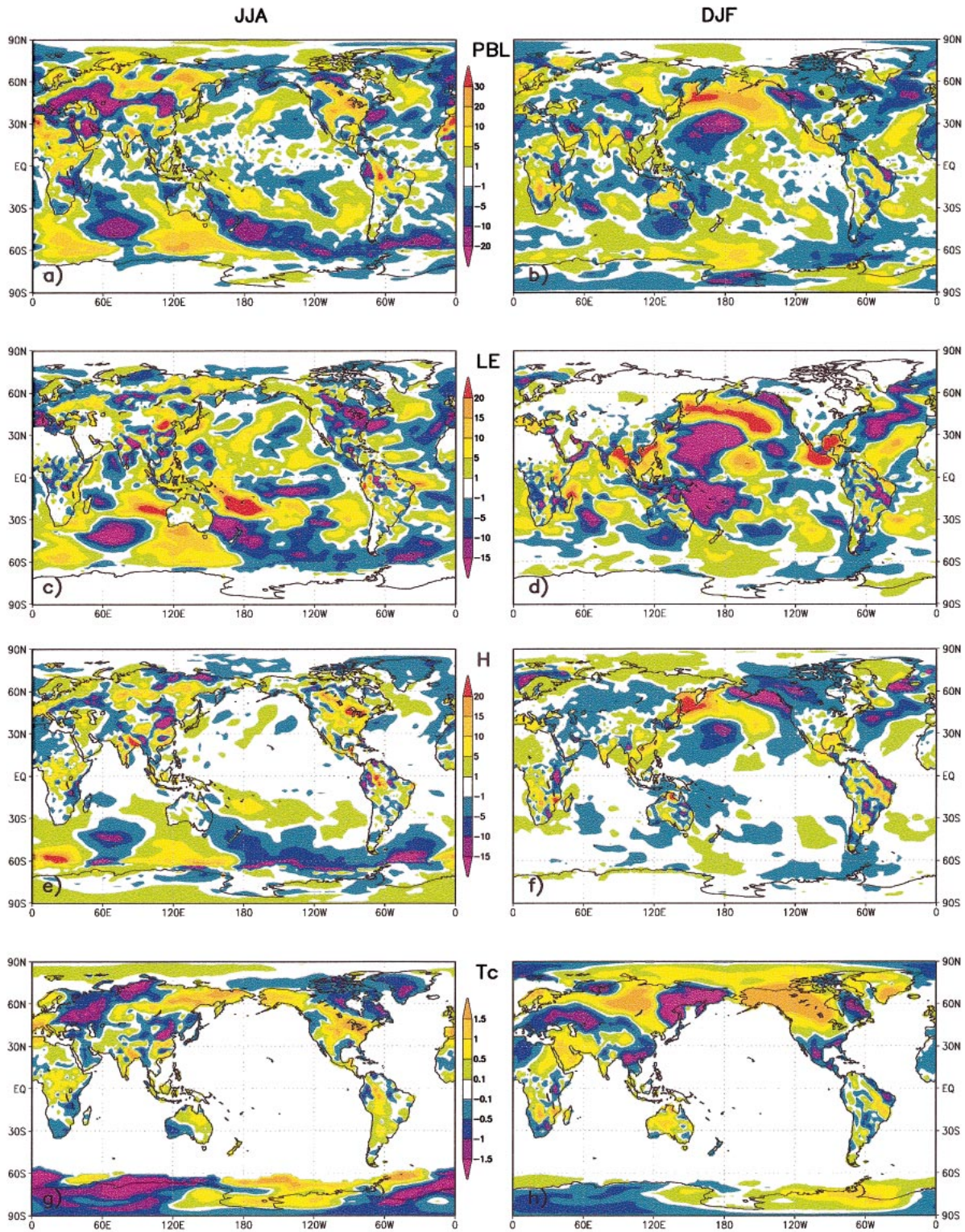


FIG. 2. (a) JJA ensemble mean PBL height EM - M difference in mb (1 mb \approx 10 m near the surface). Contour shading is as indicated on the color bar. (b) Same as in (a) but for DJF. (c) JJA ensemble mean latent heat flux EM - M difference in $W m^{-2}$. (d) Same as in (c) but for DJF. (e) JJA ensemble mean sensible heat flux EM - M difference in $W m^{-2}$. (f) Same as in (e) but for DJF. (g) JJA ensemble mean canopy temperature EM - M difference in K. (h) Same as in (g) but for DJF.

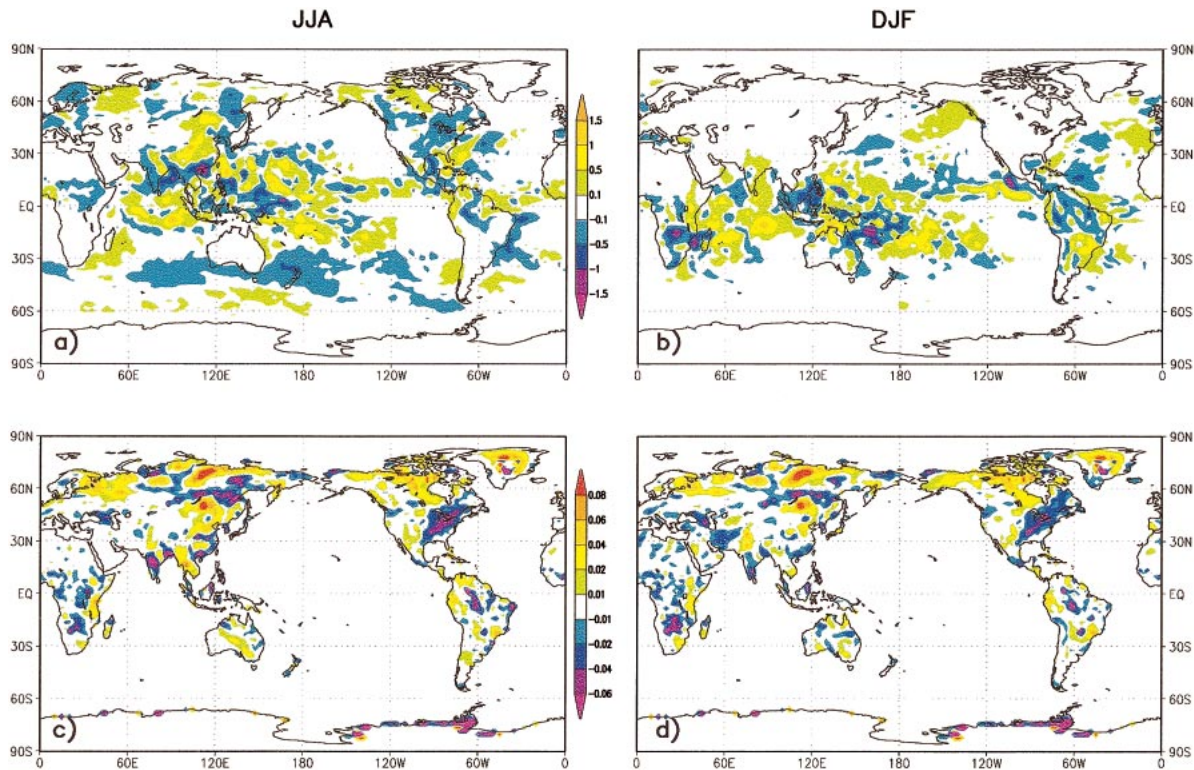


FIG. 3. (a) JJF ensemble mean convective precipitation EM - M difference in mm day^{-1} . Contour shading is as indicated on the color bar. (b) Same as in (a) but for DJF. (c) JJA ensemble mean deep soil moisture EM - M difference in fraction of field capacity. (d) Same as in (c) but for DJF.

field, indicating the locations and extent to which the boundary layer air has been vented to the free atmosphere. Because of the substantial differences in characteristics of boundary layer air and tropospheric air, frequent occurrence of the exchange has the potential to substantially alter the climate of the troposphere. Another link between the boundary layer and the climate is the impact of the short time-scale processes associated with boundary layer turbulence on the relatively low frequency phenomena in the soil system. The deep soil moisture, or the soil moisture in the layer below the root zone, specified in the land surface model as a function of vegetation type, varies on time scales ranging from weekly to annual and interannual (Wu et al. 2002). Ensemble mean differences between the EM and M simulations, which were initialized with the same deep soil moisture and temperature, indicate the communication of the differences due to modeling technique to the longer time-scale properties of the mean climate (Findell and Eltahir 2003). The EM - M ensemble and seasonal mean differences of convective precipitation and deep soil moisture are shown in Figs. 3a-d.

The magnitude of the EM - M differences in convective precipitation (Figs. 3a and 3b) generally follows the magnitude of the precipitation field itself, with the largest differences occurring in the intertropical convergence zone, the South Pacific convergence zone, and

the monsoon regions in India and Asia in JJA and in Australia in DJF. The EM - M differences are up to $1\text{--}1.5 \text{ mm day}^{-1}$ in oceanic regions where the mean convective precipitation is up to 8 mm day^{-1} , and over land areas where the convective precipitation is up to 4 mm day^{-1} . The relatively small scale structures with alternating signs in the difference field over the oceans indicate shifts in the centers of precipitation rather than systematic changes in the amount of precipitation. The level of significance of these differences was generally lower (closer to 70%) than the differences over the continents. Over the land areas, there is a general trend toward negative EM - M differences, meaning smaller precipitation in EM, with an exception in the area of northern China and Mongolia in JJA. The areas where the largest differences in the boundary layer structure occurred, such as the eastern United States, show some difference in precipitation, but those are not the regions where the differences in precipitation are largest, except again for the region in east-central Asia. The contrast between the behavior over the United States and northern China will be discussed in section 4.

The EM - M differences in the deep soil moisture, Figs. 3c and 3d, reflect an integrated effect of the precipitation differences over the land, and therefore are large where the precipitation differences are large, or where the precipitation differences are persistent. The

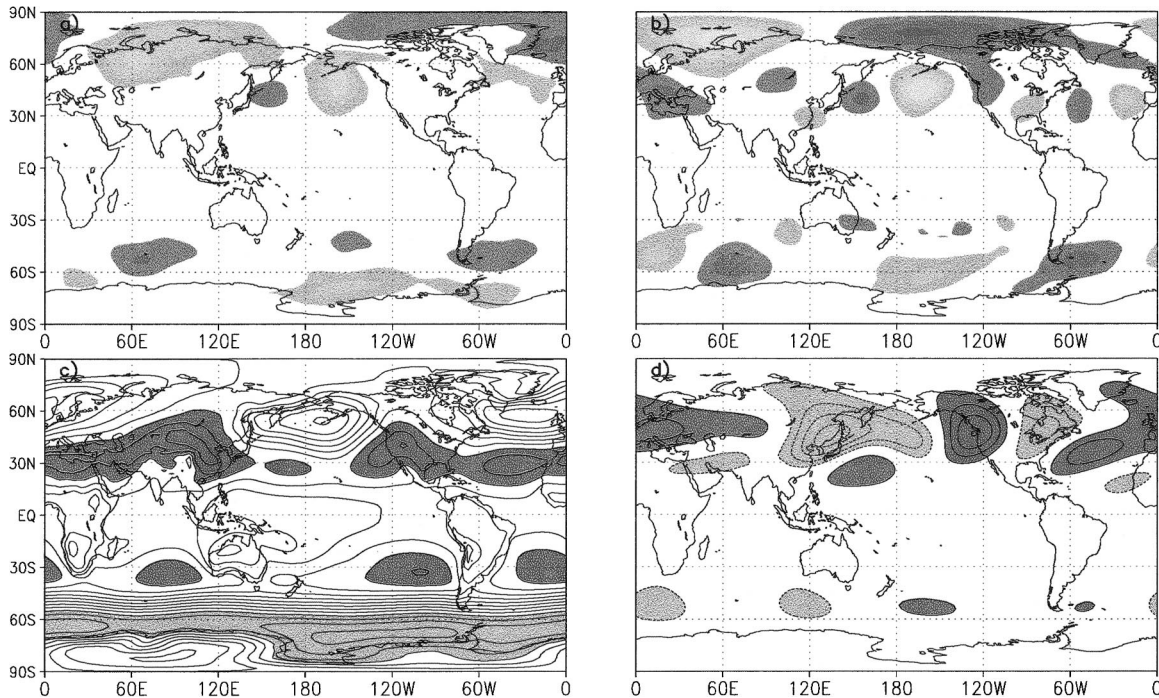


FIG. 4. (a) DJF ensemble mean EM - M sea level pressure difference in mb. Contour interval is 1 mb, dark gray shading is for differences less than -1 mb, and light gray shading is for differences greater than 1 mb. (b) DJF ensemble mean EM - M 300-mb eddy height differences in m. Contour interval is 10 m, dark gray shading is for differences less than -10 m, and light gray shading is for differences greater than 10 m. (c) EM sea level pressure in mb. Contour interval is 4 mb, dark gray shading is for pressures below 988 mb, and light gray shading is for pressures above 1020 mb. (d) Ensemble mean 300-mb eddy height in m. Contour interval is 60 m, dark gray shading indicates eddy heights less than -60 m, light gray shading indicates heights greater than 60 m.

regions where this integrated effect is most apparent are east-central Asia, where the deep soil moisture is wetter in the EM simulation, and over the eastern United States, north-central Asia, and the Indian subcontinent, where the deep soil moisture is drier. The striking similarity of the DJF and JJA difference fields shown in the figures is an indicator of the annual (or longer) time scale on which the deep soil moisture varies in the GCM.

c. Impact on the mean circulation

The impact on the atmospheric circulation of the modeling choice may be assessed by examining the zonal and seasonal means of the temperature or horizontal components of the wind, as well as the zonally integrated mass streamfunction, a measure of the strength of the Hadley circulation. The EM and M simulations show very little difference in these measures of the zonal mean climate. The ensemble mean stationary wave pattern, however, does exhibit some change due to the choice of land-atmosphere coupling technique. This impact is manifest directly in the seasonal mean deviation from the zonal mean meridional transport of heat or momentum, and also in the seasonal mean sea level pressure (SLP) field and 300-mb eddy height (deviation from the zonal mean geopotential height) field.

The DJF seasonal mean sea level pressure field for

the EM - M differences and for the EM simulation alone are shown in Figs. 4a and 4c, respectively. Similar spatial patterns are seen in the 300-hPa eddy height field, again from EM - M difference and for EM alone, shown in Figs. 4b and 4d. The pattern of alternating troughs and ridges in the DJF EM eddy height field (Fig. 4d), shown by alternating centers of light gray (ridge) and dark gray (trough) beginning with the ridge in the central Pacific and continuing into the northern Pacific and over the North American continent into the Atlantic, is the Pacific-North America (PNA) pattern of variability, defined originally by Wallace and Gutzler (1981). The mechanism suggested to explain the presence of this stationary pattern in wintertime is the excitation of Rossby waves in the subtropics and their propagation into higher latitudes (see, e.g., Trenberth et al. 1998). The difference field (Fig. 4b) has a large negative center in the northern Pacific region where the eddy height has a trough, and a positive center over the North American west coast where the eddy height has a ridge. There is a shadow of this pattern of negative EM - M difference over troughs and positive difference over ridges across the North American continent into the Atlantic. This illustrates the strengthening of the PNA pattern of variability in the EM simulation. This result suggests that the manner in which land surface heterogeneities are modeled may exert an influence on

the PNA pattern. The possible influence of the land surface hydrology on the amplitude of the PNA has been reported by Trenberth et al. (1998) in a study based on observations and model results, although no specific mechanism was suggested. Also, Werth and Avissar (2002), in their study of the teleconnection patterns in European climate generated by Amazonian deforestation, suggest that planetary-scale Rossby waves may indeed be excited due to processes that occur at the land surface, related to changes in landscape.

4. Results: Regional perspective

We now examine in more detail several regions around the globe that illustrate the EM – M differences in boundary layer structure, links to the mean climate, and the mean climate itself. The differences over the eastern United States in summertime and an opposite pattern of behavior over northern China in summertime are presented here to illustrate the EM – M differences in boundary layer structure. The differences over Australia during the monsoon are presented to illustrate the connection between the behavior of the boundary layer structure and the precipitation, and the differences in ground temperature over the western United States and Canada are presented to illustrate the local impact of changes in the global circulation.

The sensitivity of the canopy temperature and local climate in the eastern United States in the earlier GCM simulations is consistent with the results of the offline study described in Molod and Salmun (2002), where it was shown that canopy temperature differences during summertime in mesothermal moist climates are controlled by differences in latent heat flux. In that study the canopy temperature was strongly influenced by the increased tile-to-tile variability in mosaic, and in particular by the extent to which the reduced evaporation over the bare soil component of the grid box is represented in the grid average.

A graphical summary of the behavior of the ensemble mean differences between EM and M over the eastern United States is shown in Fig. 5. The EM – M differences in JJA show that the EM simulation has a higher canopy temperature (Fig. 5a), more sensible heat flux (Fig. 5b), higher eddy diffusion coefficient near its maximum level at 900 mb (Fig. 5d), and higher temperature near the top of the PBL at 850 mb (Fig. 5f). The related behavior of the hydrological cycle shows that in the EM simulation there is less evaporation (Fig. 5c), lower relative humidity (RH) at 850 mb (Fig. 5h), slightly less precipitation (Fig. 5g), and lower soil moisture in the shallow layer (Fig. 5e). The causal relationships among these differences can be inferred using physically based arguments. For instance, higher canopy and air temperature at 850 mb could lead to lower relative humidity and so less precipitation. This potential connection between the energy budget at the surface and the hydrological cycle was demonstrated by Cook (1994) based

on results from a linearized primitive equation model used to study precipitation patterns in Africa.

A positive feedback loop suggests itself here, beginning at any panel in Fig. 5 and progressing clockwise around the panels in the figure. This loop, as is manifest over the eastern United States, is illustrated schematically in Fig. 6 by the circular path on the left. Starting with Fig. 5a and at the bottom of the left circle in Fig. 6, warmer temperatures lead to more eddy diffusion and sensible heat flux, generating warmer temperatures aloft and therefore lower relative humidity. This, in turn, results in less precipitation and less moisture input into the soil and so a drier shallow soil layer. Less soil moisture available results in lower evaporation, and less cooling at the ground due to latent heating results in a warmer canopy temperature. This feedback loop could be initiated at any point. An hypothesis for the starting point of this loop, and the connection between the differences imposed directly by using EM as opposed to M and the observed differences in the simulated climate will be presented in the next section.

The type of causality suggested in the feedback loop described here is difficult to establish unambiguously, but some causal relationships can be argued based on computed correlations between fields and some physical reasoning. A causal connection of this sort can be established between the latent heat flux, the canopy temperature, and the sensible heat flux. This relationship is investigated here by examining the correlation between the monthly mean EM – M differences in canopy temperature and latent heating. The correlation coefficient of the monthly mean EM – M differences in canopy temperature, T_c , and evaporation, LE, is shown in Fig. 7a. The physical relationship between T_c and LE is such that evaporation increases with temperature, and also that evaporation acts to cool the surface. A large positive correlation therefore suggests that the canopy temperature difference would explain the difference in evaporation, whereas a large negative correlation suggests that the evaporation difference explains (part of) the difference in canopy temperature. The large negative area in the center of the North American continent suggests that the positive EM – M difference in canopy temperature (seen in Fig. 5) is a result of the decreased evaporation in EM relative to M. This relationship is also consistent with the offline results from Molod and Salmun (2002). A similar argument can be made about the sign of the correlation between sensible heat and canopy temperature differences. The sensible heat increases with canopy temperature, and the sensible heating will act to cool the surface. The correlation coefficient of the ensemble mean EM – M differences in sensible heat and T_c , shown in Fig. 7b, is generally positive in the location where the summertime differences occur, suggesting that the larger sensible heating is a result of the warmer temperatures.

A similar feedback pattern to the one described by the left circle in Fig. 6 exists over northern China and

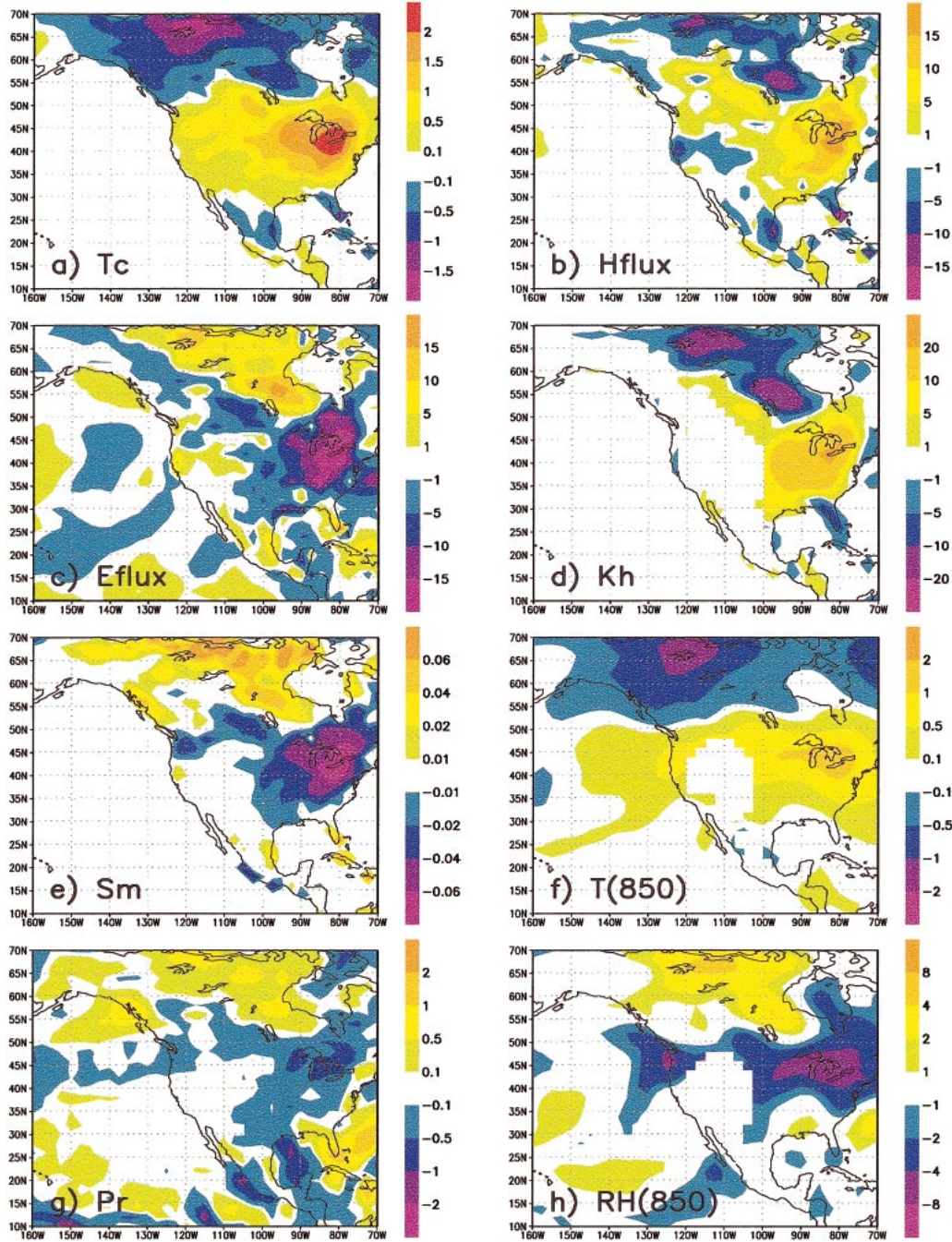


FIG. 5. JJA ensemble mean EM - M difference over the United States and parts of Canada of (a) canopy temperature in K, (b) sensible heat flux in $W m^{-2}$, (c) latent heat flux in $W m^{-2}$, (d) eddy diffusion coefficient for heat in $m^2 s^{-1}$, (e) shallow zone soil moisture in fraction of field capacity, (f) temperature at 850 mb in K, (g) total precipitation in $mm day^{-1}$, and (h) relative humidity at 850 mb. Contour levels are as indicated on the color bars next to each panel.

Mongolia in JJA, but the initial feedback here is negative, and the feedback loop is in the opposite sign. This pattern is illustrated schematically by the right circle in Fig. 6, and can be seen by the patterns over northern China in Figs. 2 and 3. Beginning at the bottom of the right-hand loop in the schematic, cooler canopy tem-

peratures are associated with cooler temperatures aloft and higher relative humidity. This, in turn, generates more precipitation, wetter soils, and higher evaporation, and the higher evaporation cools the soil and results in cooler temperatures. An explanation for the presence of this opposite phase of the summertime feedback pattern

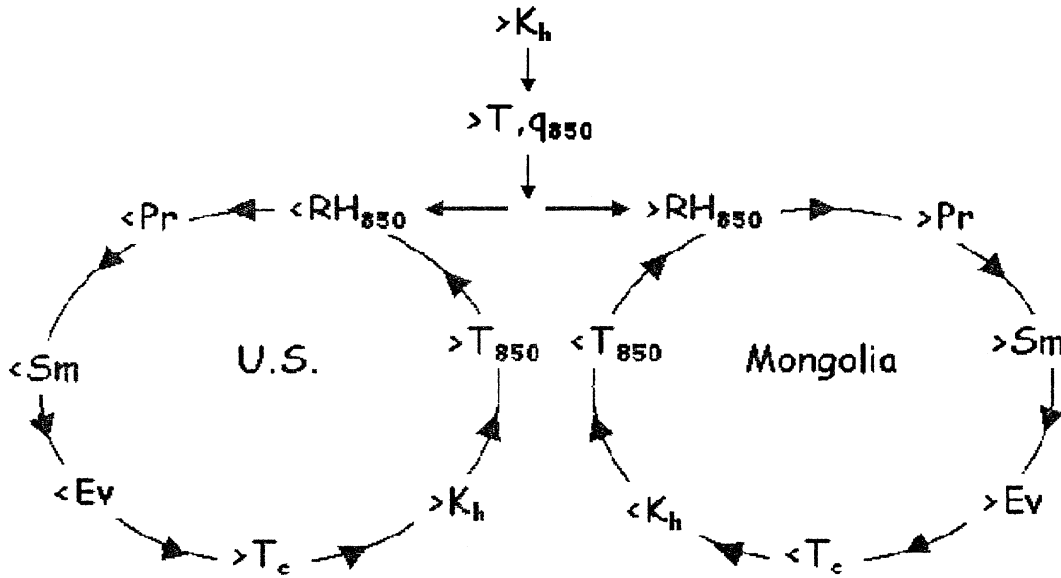


FIG. 6. Schematic of the suggested feedback loop illustrating (top center) the direct changes due to using EM, (left) the positive feedback as is manifest in the summertime over the eastern United States, and (right) the opposite-sign feedback as is manifest over northern China and Mongolia. The symbols in the schematic are defined as follows: RH_{850} and T_{850} are the relative humidity and temperature at the 850-mb level, respectively; Pr is the precipitation; S_m is the soil moisture; Ev is the evaporation; T_c is the canopy temperature; and K_h is the eddy diffusivity for heat and moisture.

is associated with the presence of a deciduous forest over northern China, and will be discussed in more detail in the next section.

Another region of the globe that exhibited large EM – M differences, particularly in PBL height and precipitation, is the region of the Australian monsoon during DJF. The EM – M differences in DJF monthly mean precipitation and PBL height over Australia are shown in Fig. 8. The EM simulation has larger precipitation amounts over the northern land areas, and less over the ocean (Fig. 8a). This constitutes an increased excursion of the monsoon precipitation over the land. Figure 8b

shows that the PBL height is lower in EM in the regions where the precipitation is higher. This connection in EM between lower boundary layer heights over wetter, cooler areas, and increased precipitation due to higher equivalent potential temperature, is similar to the connection between wet domains and precipitation suggested by the work reported in Cotton and Pielke (1992). This behavior demonstrates a mechanism by which the local impact of modeling differences impacts the free atmosphere and so may affect the mean climate elsewhere.

The final regional behavior to be discussed in this section illustrates the local impact of changes in global

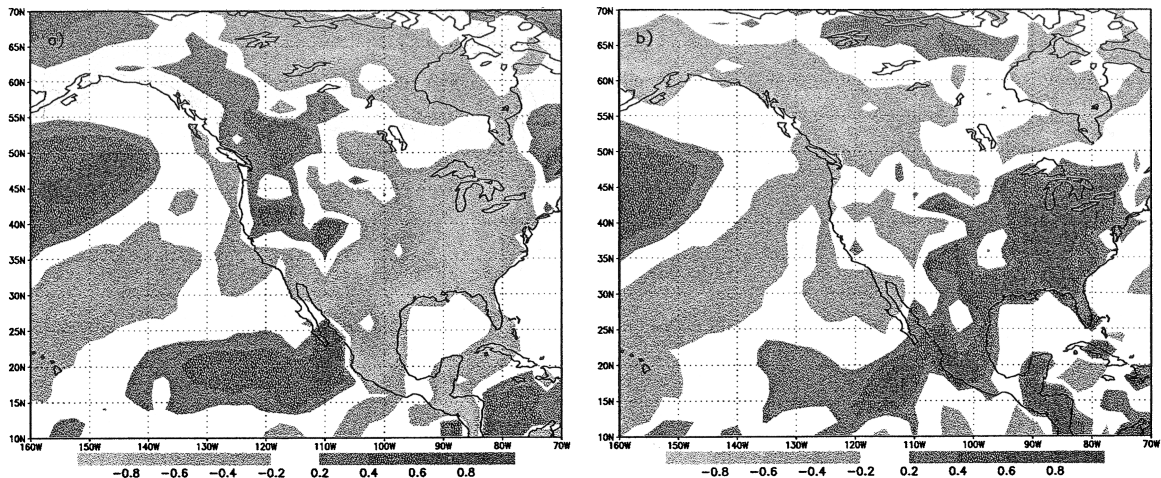


FIG. 7. Correlation coefficient of the monthly mean EM – M differences in (a) canopy temperature and latent heat flux, and (b) canopy temperature and sensible heat flux.

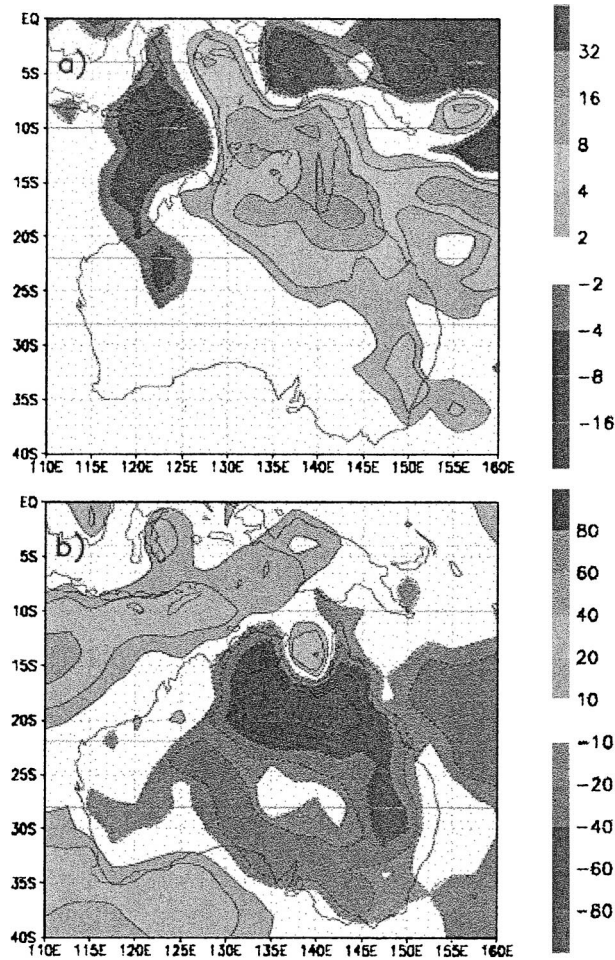


FIG. 8. (a) Jan avg difference (EM – M) in precipitation in mm day^{-1} over Australia. (b) Jan avg difference PBL thickness in mb.

circulation generated by the difference in modeling technique. Examination of Fig. 2h reveals a pattern of large EM – M differences in canopy temperature in DJF over the northwestern United States and western Canada. The EM simulation produces canopy temperatures that are up to 1.5–2 K warmer than the M simulation. There is some contribution to the relative cooling in M from a decrease in downward sensible heat flux, as is suggested by the relatively high negative correlation between differences in sensible heat flux and canopy temperature over those regions, shown in Fig. 7. However, a connection also exists between the warmer canopy temperatures in EM and the increased amplitude of the PNA pattern which was shown in section 3. It has been shown by Koide and Kodera (1999), using singular value decomposition of the surface temperature, that the PNA mode describes a significant amount of variability in the surface temperature over the North American continent, and the connection is such that a stronger PNA is associated with warmer canopy temperatures in western Canada. The canopy temperature pattern of EM – M

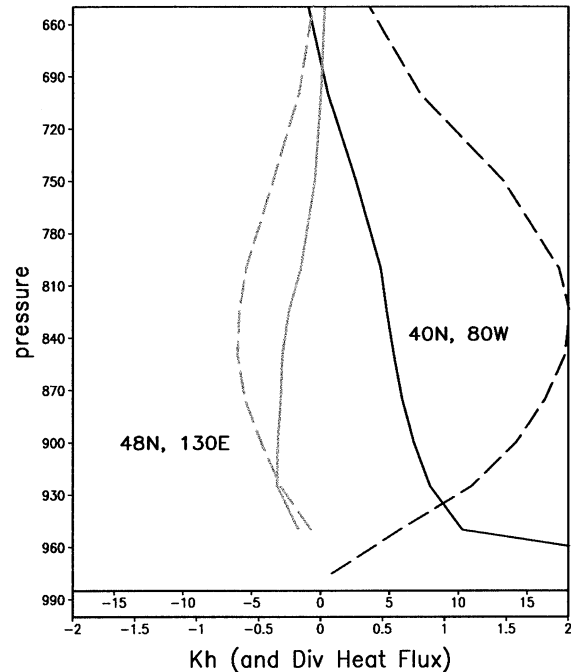


FIG. 9. Grid-averaged ensemble mean EM – M difference during JJA of the divergence of the turbulent heat flux in K s^{-1} (solid line) and eddy diffusion coefficient in $\text{m}^2 \text{s}^{-1}$ (dashed line) as a function of atmospheric pressure in mb. The lower axis shows the scale for the divergence of the flux, and the upper axis shows the scale for the diffusion coefficient. The profiles shown are for one point in the eastern United States (black) and one point in Mongolia (gray).

differences shown in Fig. 2h, therefore is a response to both local (sensible heating) and remote (PNA) processes.

5. Discussion

The central issue that distinguishes the EM technique from the standard mosaic technique is the behavior of the turbulent diffusion in the boundary layer over a heterogeneous terrain. The EM technique retains the tile-to-tile differences up to the level dictated by the local conditions. The M technique, however, removes all tile-to-tile variability above the surface layer. This increased (tile to tile) variance on scales smaller than a grid box serves to increase the turbulent kinetic energy and turbulent fluxes as a direct result of modeling the land surface–atmosphere coupling with EM. This enhancement of the turbulent diffusion as a direct impact of EM will provide some explanation for the behavior of the GCM EM – M differences.

Individual ensemble mean JJA profiles of the eddy diffusion coefficient for heat and moisture in the GCM, and the corresponding divergence of the turbulent heat flux are shown in Fig. 9. The profiles from 40°N, 80°W typify the behavior over the eastern United States, southern Africa, and the other regions that exhibit the pattern shown in Fig. 5 in summertime. The positive

value of the EM – M difference of the turbulent heat flux divergence (solid black line) and eddy diffusion coefficient (dashed black line) seen in the figure demonstrates the enhanced diffusion of heat and the enhanced eddy coefficient. The climate feedback simulated in this region serves to reinforce the direct effect of EM which is to enhance the eddy diffusion. This reinforcement of the initial effect ensues as the enhanced vertical diffusion of heat in EM over this region results in warmer air aloft, lower relative humidity, less precipitation, soil moisture, and evaporation, and warmer ground temperatures which generate higher eddy diffusion coefficients (associated here with higher diffusion). This is the positive feedback pattern described in Fig. 5 and in the schematic at the left side of Fig. 6. This feedback is likely to have been initiated by the larger eddy diffusion due to the EM technique. This initiation is depicted by the top center section of the schematic of Fig. 6.

Figure 9 also shows profiles from 48°N, 130°E that typify the behavior over northern China and Mongolia. These profiles show a pattern of EM – M differences opposite in sign to the pattern seen in the eastern United States. This behavior, however, may also be understood in the context of the direct effect of the EM formulation to enhance the diffusion. The different manifestation of the impact of EM on the simulated climate is related to the water balance near the surface. Figure 10 shows the latent heat flux in JJA (from the EM simulation) as well as the evaporative fraction, indicating an important difference between the eastern United States and northern China that affects the response to EM. The seasonal mean evaporation over the northern China region is approximately 90 W m^{-2} , and over the U.S. region closer to 60 W m^{-2} . The importance of the surface flux of moisture relative to the surface flux of heat is also illustrated in Fig. 10b, where the evaporative fraction (latent/latent + sensible) is nearly 0.8 in northern China and closer to 0.5 over the eastern United States. This difference in the importance of the surface evaporation is associated with the presence of a broadleaf deciduous forest in the northern China region.

As argued earlier, the direct effect of EM is to enhance the diffusion of moisture as well as heat. In contrast to the behavior over the eastern United States, the result in this region with its higher evaporative fraction is to *increase* the relative humidity aloft. This occurs due to the dominance of the moisture effect (to increase RH) over the temperature effect (to reduce RH). This increase in relative humidity aloft then initiates the pattern of behavior shown in the right side of Fig. 6. The increased diffusion (black) results in an increased relative humidity in EM, an increased precipitation, soil moisture, and evaporation (these can all be seen in the region of northern China in Figs. 3a, 3c, and 2c), a decreased canopy temperature (Fig. 2g), and a resulting *decrease* in the eddy diffusion coefficient, K_h . The direct response, therefore, to the enhanced diffusion due to EM

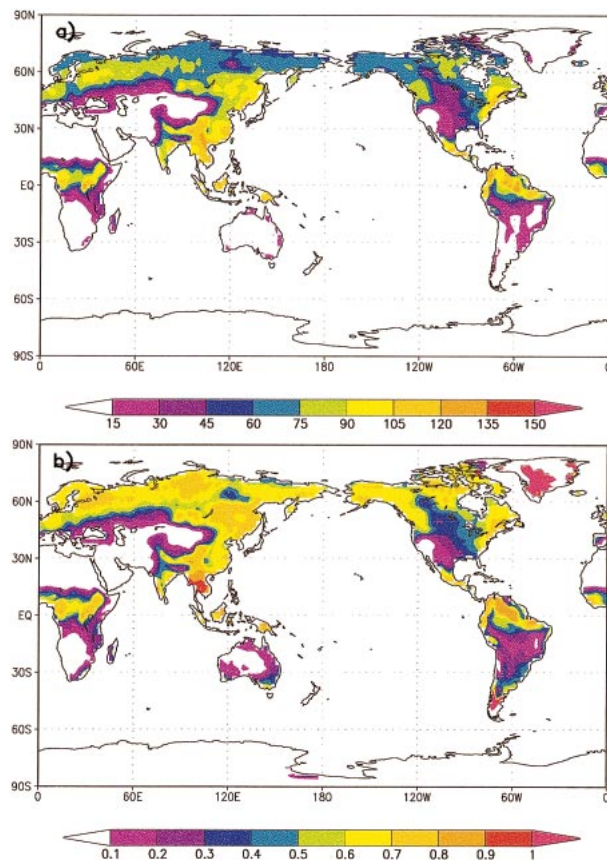


FIG. 10. (a) Ensemble mean latent heat flux for JJA in W m^{-2} from the EM simulation. (b) Evaporative fraction for the same period, defined as the ratio of the latent heat flux to the sum of the latent and sensible heat fluxes.

is a negative feedback that acts to *suppress* the turbulent diffusion.

The enhanced evaporation in EM, however, acts as a ground source for the turbulent flux. This overrides the reduction in moisture diffusion that would be implied by the reduced eddy diffusion coefficient, and the result is an enhanced moisture diffusion. This is illustrated by the increased divergence of the turbulent moisture flux (positive EM – M difference) for 48°N, 130°E, of Fig. 11 (gray curve). The enhanced moisture diffusion in the EM simulation near the surface in the northern China region contributes to an increase in the boundary layer relative humidity, and the feedback pattern ensues, with increased precipitation, soil moisture, and evaporation, which results in a higher moisture diffusion. The completion of this feedback loop is depicted by the left-hand side of the cycle shown at right in Fig. 6.

The lower canopy temperature and sensible heat flux seen in the climate of this region is a result of the behavior of the hydrological cycle. The Bowen ratio (or the evaporative fraction) therefore dictates the sign of the positive feedback that determines the mean climate impact of EM. The enhanced diffusion due directly to

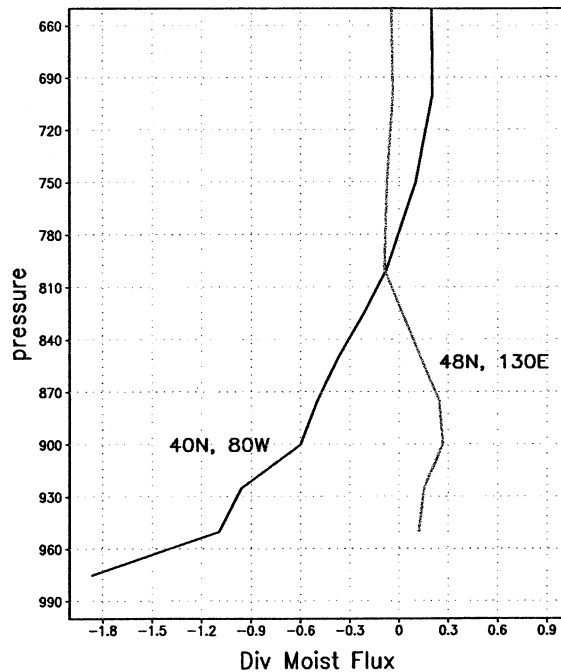


FIG. 11. Grid-averaged ensemble mean EM - M difference during JJA of the divergence of the turbulent moisture flux in $\text{g kg}^{-1} \text{s}^{-1}$ as a function of atmospheric pressure in mb. The profiles shown are for one point in the eastern United States (black) and one point in Mongolia (gray).

the EM technique serves to suggest how the pattern began, and the dominance of either the sensible or latent heat transfer in the local climate determines how the impact of EM is manifest over a relatively drier (eastern United States) versus a wetter (eastern China) region.

6. Summary

Two 10-yr-long simulations were performed with the GEOS GCM to evaluate the impact on the resulting climate of using the extended mosaic technique rather than a mosaic technique to couple the heterogeneous land surface and the atmosphere. The results of these side-by-side simulations showed statistically significant differences on local and global scales, and demonstrate that extending the direct influence of subgrid-scale heterogeneities upward into the boundary layer using EM has the potential to affect the modeled climate.

The impact on the local boundary layer structure of using EM was evaluated by examining the EM - M ensemble and seasonal mean differences in planetary boundary layer height, sensible and latent heat fluxes, and canopy temperature. The largest differences were on the order of 10% of the mean field value, generally in summertime in both hemispheres. Particular attention was focused on the differences over the eastern United States and eastern Asia in JJA, and southern Africa in DJF. These focus regions also exhibited EM - M differences in the fields that represent the links between

the boundary layer and the mean climate; that is, the convective precipitation and the deep soil moisture, and a positive feedback loop were identified to explain the behavior over these regions.

The planetary boundary layer depth, sensible heat flux, and canopy temperature are all higher in EM over the eastern United States, southern Africa, and southeast and northeast Asia, where the latent heat flux and the convective precipitation are lower. The causality of this pattern of differences was elucidated by arguing that the eddy diffusion is enhanced in EM relative to M as a direct result of the change in technique. This suggested that in these regions, the enhanced eddy diffusion of heat and moisture, which would generate higher temperatures and humidities aloft in the boundary layer, caused the initiation of a feedback pattern that resulted in the observed systematic pattern of ensemble mean differences. In these regions, whose behavior was illustrated with the results over the eastern United States, the higher boundary layer temperature resulted in a lower relative humidity at those levels, and the suppression of the precipitation. The lower precipitation resulted in drier soils and less evaporation, which acted to warm the canopy temperatures. The warmer skin temperatures, in turn, generated higher sensible heat flux and higher eddy diffusion. This completed the positive feedback.

A pattern of opposite sign was seen over a region in northern China and Mongolia, where the PBL depth, canopy temperature, and sensible heat fluxes were all lower in EM, and the precipitation and evaporation were higher. In this region, the feedback pattern is manifest in connection with the higher mean evaporation rates over the deciduous forest. The enhanced eddy diffusion that results directly from the EM formulation enhances the temperature and humidity aloft, as occurs in the eastern United States. The dominant role played by the moisture diffusion in this region, however, results in a higher relative humidity aloft, and enhances the precipitation in the EM simulation. This initiates the positive feedback of opposite sign.

An impact of EM on the mean circulation was also evident in the results, as demonstrated by the EM - M differences in the 300-mb eddy height. The seasonal mean deviation from the zonal mean geopotential height is an indicator of the stationary wave pattern in the atmosphere, and is used to detect the Pacific-North America pattern of variability. The PNA pattern was strengthened in the EM simulation relative to M, although no clear mechanism for this influence was apparent. The strengthening of the PNA in EM was also connected to a pattern of warmer wintertime canopy temperatures in EM in the western North American continent.

The analysis and synthesis of GCM results presented here has centered on a discussion and account of the sign of the EM - M differences. The magnitude of the EM - M differences in the GCM simulations must be understood as well. A preliminary step is to examine

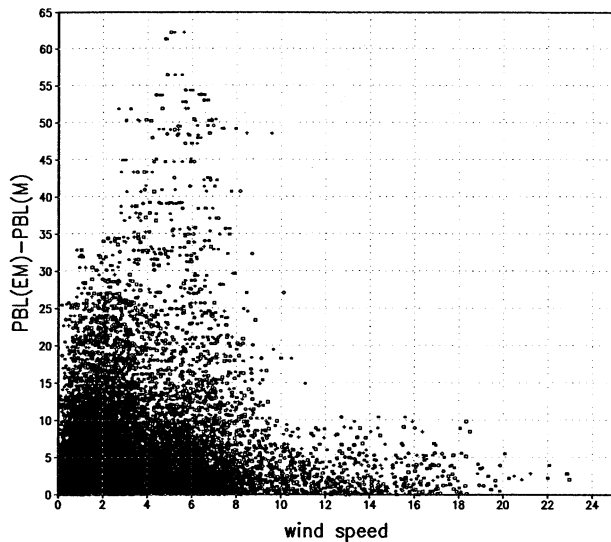


FIG. 12. Scatter diagram of the JJA ensemble mean EM – M difference in PBL height in mb and the wind speed at 900 mb in m s^{-1} from the EM simulation.

scatter diagrams of the differences in PBL height, for example, between the EM and M experiments, and relevant grid-scale or tile-scale parameters. In an observational study by Banta and White (2003), it was found that the difference in PBL heights over nearby terrains with differences in underlying vegetation was strongly dependent on the prevailing magnitude of the boundary layer winds. Strong winds were observed to suppress any terrain-related differences. A scatter diagram to illustrate the dependence of the ensemble mean EM – M PBL height difference on the winds from 900 to 950 mb is shown in Fig. 12. The large spread of values in the scatter diagram demonstrates that there are other factors involved in determining the PBL height differences, but the largest PBL height differences are clearly associated with wind speeds near 6 m s^{-1} , and the differences clearly diminish as the wind speed increases. This suggests that the magnitude of the EM – M differences seen here are related to the magnitude of the background wind, and are larger when the advective influence of the mean wind is smaller. Further examination of the relationships between the magnitude of the EM – M differences and the background state of the atmosphere as well as other land surface fields is warranted. This work will include elucidating the role of the background profiles of temperature and humidity, as well as the role of the turbulent kinetic energy.

The results reported here have demonstrated clearly that the use of EM impacts the simulated climate. The behavior of EM versus M must still be evaluated, however, in comparison with satellite-derived and in situ estimates of the climate to assess whether any of these differences constitute an improved simulation. Comparisons of this sort will also provide an assessment of the circumstances and conditions under which the ex-

tended mosaic technique provides the GCM with a better description of the land–atmosphere coupling. The different elements of the positive feedback mechanism described in this study must also be evaluated, initially using reanalysis data, to bolster the argument that this mechanism is relevant and important in the climate system, and that a GCM that allows this mechanism to occur can provide improved simulations.

REFERENCES

- Angevine W. M., A. B. White, C. J. Senff, M. Trainer, R. M. Banta, and M. A. Ayoub, 2003: Urban–rural contrasts in mixing height and cloudiness over Nashville in 1999. *J. Geophys. Res.*, **108**, 4092, doi:10.1029/2001JD001061.
- Arola, A., 1999: Parameterization of turbulent and mesoscale fluxes for heterogeneous surfaces. *J. Atmos. Sci.*, **56**, 584–598.
- Banta, R. M., and A. B. White, 2003: Mixing-height differences between land use types: Dependence on wind speed. *J. Geophys. Res.*, **108**, 4321, doi:10.1029/2002JD002748.
- Bringfelt, B., M. Heikinheimo, N. Gustafsson, V. Perov, and A. Lindroth, 1999: A new land-surface treatment for HIRLAM—Comparisons with NOPEX measurements. *Agric. For. Meteorol.*, **98–9**, 239–256.
- Cook, K. H., 1994: Mechanisms by which surface drying perturbs tropical precipitation fields. *J. Climate*, **7**, 400–413.
- Cotton, W. R., and R. A. Pielke, 1992: *Human Impacts on Weather and Climate*. Cambridge University Press, 288 pp.
- Ducoudre, N. I., K. Laval, and A. Perrier, 1993: SECHIBA, a new set of parameterizations of the hydrologic exchanges at the land–atmosphere interface within the LMD atmospheric general circulation model. *J. Climate*, **6**, 248–273.
- Findell, K., and E. Eltahir, 2003: Atmospheric controls on soil moisture–boundary layer interactions. Part II: Feedbacks within the continental United States. *J. Hydrometeorol.*, **4**, 573–583.
- Gates, W. L., Ed., 1995: *The Proceedings of the First International AMIP Scientific Conference*. WCRP-92, WMO/TD-No. 732, World Climate Research Programme, World Meteorological Organization, 532 pp.
- Helfand, H. M., and J. C. Labraga, 1988: Design of a nonsingular level 2.5 second-order closure model for the prediction of atmospheric turbulence. *J. Atmos. Sci.*, **45**, 113–132.
- , and S. D. Schubert, 1995: Climatology of the simulated Great Plains low-level jet and its contribution to the continental moisture budget of the United States. *J. Climate*, **8**, 784–806.
- , A. Molod, and M. G. Bosilovich, 1999: Implications of a moist turbulence parameterization for the numerical prediction of the structure and properties of the atmospheric boundary layer. Preprints, *13th Conf. on Numerical Weather Prediction*, Denver, CO, Amer. Meteor. Soc., 54–59.
- Hubbe, J. M., J. C. Doran, J. C. Liljegren, and W. J. Shaw, 1997: Observations of spatial variations of boundary layer structure over the Southern Great Plains Cloud and Radiation Testbed. *J. Appl. Meteorol.*, **34**, 1221–1231.
- Koide, H., and K. Kodera, 1999: A SVD analysis between the winter NH 500-hPa height and surface temperature fields. *J. Meteor. Soc. Japan*, **77**, 47–61.
- Koster, R. D., and M. J. Suarez, 1992a: Modeling the land surface boundary in climate models as a composite of independent vegetation stands. *J. Geophys. Res.*, **97**, 2697–2715.
- , and —, 1992b: A comparative analysis of two land surface heterogeneity representations. *J. Climate*, **5**, 1379–1390.
- , and —, 1992c: Energy and water balance calculations in the MOSAIC LSM. NASA Tech. Memo. 104606, Technical Report Series on Modeling and Data Assimilation, Vol. 9, Goddard Space Flight Center, 76 pp.
- Mahrt, L., 2000: Surface heterogeneity and vertical structure of the boundary layer. *Bound.-Layer Meteorol.*, **96**, 33–62.

- Mölders, N., A. Raabe, and G. Tetzlaff, 1996: A comparison of two strategies on land surface heterogeneity used in a mesoscale β meteorological model. *Tellus*, **48A**, 733–749.
- Molod, A., and H. Salmun, 2002: A global assessment of the mosaic approach to modeling land surface heterogeneity. *J. Geophys. Res.*, **107**, 4217, doi:10.1029/2001JD000588.
- , —, and D. W. Waugh, 2003: A new look at modeling surface heterogeneity: Extending its influence in the vertical. *J. Hydro-meteor.*, **4**, 810–825.
- Reynolds, R. W., 1988: A real-time global sea surface temperature analysis. *J. Climate*, **1**, 75–86.
- Rosenzweig, C., and F. Abramopoulos, 1997: Land-surface model development for the GISS GCM. *J. Climate*, **10**, 2040–2054.
- Trenberth, K. E., G. W. Branstator, D. Karoly, A. Kumar, N.-C. Lau, and C. Ropelewski, 1998: Progress during TOGA in understanding and modeling global teleconnections associated with tropical sea surface temperatures. *J. Geophys. Res.*, **103** (C7), 14 291–14 324.
- Vihma, T., 1995: Subgrid parameterization of surface heat and momentum fluxes over the polar oceans. *J. Geophys. Res.*, **100** (C11), 22 625–22 646.
- Wallace, J. M., D. S. Gutzler, 1981: Teleconnections in the geopotential height field during the Northern Hemisphere winter. *Mon. Wea. Rev.*, **109**, 784–812.
- Werth, D., and R. Avissar, 2002: The local and global effects of Amazon deforestation. *J. Geophys. Res.*, **107**, 8087, doi:10.1029/2001JD000717.
- Wu, M. L., S. Schubert, I. S. Kang, and D. E. Waliser, 2002: Forced and free intraseasonal variability over the South Asian monsoon region simulated by 10 AGCMs. *J. Climate*, **15**, 2862–2880.